GSta: Efficient Training Scheme with Siestaed Gaussians for Monocular 3D Scene Reconstruction

Anil Armagan[1], Albert Saà-Garriga[1], Bruno Manganelli[1], Kyuwon Kim[2], and M. Kerim Yucel[1]

[1]Samsung R&D Institute UK (SRUK), [2]Samsung Electronics

Abstract— **Gaussian Splatting (GS) is a popular approach for 3D reconstruction, mostly due to its ability to converge reasonably fast, faithfully represent the scene and render (novel) views in a fast fashion. However, it suffers from large storage and memory requirements, and its training speed still lags behind the hash-grid based radiance field approaches (e.g. Instant-NGP), which makes it especially difficult to deploy them in robotics scenarios, where 3D reconstruction is crucial for accurate operation. In this paper, we propose GSta that dynamically identifies Gaussians that have converged well during training, based on their positional and color gradient norms. By forcing such Gaussians into a *siesta* and stopping their updates (freezing) during training, we improve training speed with competitive accuracy compared to state of the art. We also propose an early stopping mechanism based on the PSNR values computed on a subset of training images. Combined with other improvements, such as integrating a learning rate scheduler, GSta achieves an improved Pareto front in convergence speed, memory and storage requirements, while preserving quality. We also show that GSta can improve other methods and complement orthogonal approaches in efficiency improvement; once combined with Trick-GS, GSta achieves up to 5× faster training, 16× smaller disk size compared to vanilla GS, while having comparable accuracy and consuming only half the peak memory. More visualisations are available at `https://anilarmagan.github.io/SRUK-GSta`.**

I. INTRODUCTION

3D reconstruction is an integral problem in computer vision, where the aim is to leverage one or multiple images of a scene/object, and lift it to 3D while representing geometry and textures faithfully. With applications in robotics [1], edge devices [2], multimedia [3] and virtual reality [4], its industrial importance has also increased over the years. Despite the recent advances in the field, 3D reconstruction is inherently an ill-posed problem, as accurate disentanglement of geometry and texture from 2D images is required, as well as an accurate back-projection of images onto a 3D space is necessary, which is inherently ambiguous.

Following the earlier photogrammetry [6] approaches, neural rendering methods have become popular for 3D reconstruction, particularly due to their success in novel view synthesis. Neural Radiance Fields (NeRF), where a scene is encoded into a small neural network, have shown promising results [7], and its variants targeting faster convergence and rendering [8]–[10] have emerged as well. Most

recently, Gaussian Splatting (GS) [5] has been proposed, where a scene is represented with many Gaussians, whose parameters are learned with gradient-based optimization. GS based methods are arguably leads the 3D representation/reconstruction technology at the moment, due to their fast rendering speed and reasonable convergence time.

Despite its success, GS suffers from several shortcomings. First, since it represents the scenes with many Gaussians, ranging up to several millions, it has large storage requirements. Second, these many Gaussians lead to high maximum memory consumption during training, limiting the feasibility of training on devices with resource constraints. In the same vein, optimization of these many Gaussians lead to a somewhat acceptable, but definitely improvable training time. Several methods have been proposed targeting these shortcomings, such as ones reducing the number of Gaussians [11]–[15], number of attributes [11], [14], [16], and directly predicting Gaussians by leveraging diffusion priors [17]. However, there is still room for improvement on multiple axes regarding efficiency as well as fidelity.

Our work aims to advance the Pareto front of efficiency in Gaussian Splatting methods, aiming to improve training time, storage and memory requirements, while keeping the accuracy competitive. First, based on the observation that each Gaussian has different convergence traits during training
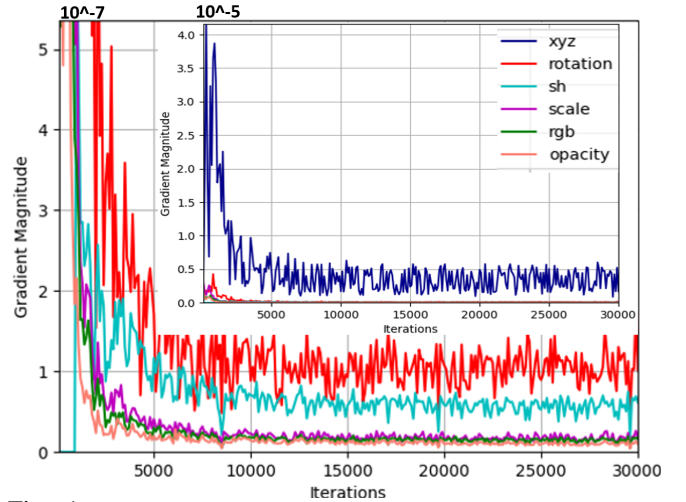

Fig. 1: Mean gradient magnitude of Gaussians during 30000 iterations of training. Training takes 6× longer since hard-coded number of training iterations in 3DGS [5], while a high number of Gaussians are converged in early iterations. Please note the scale difference between the positional and rest of the parameters.
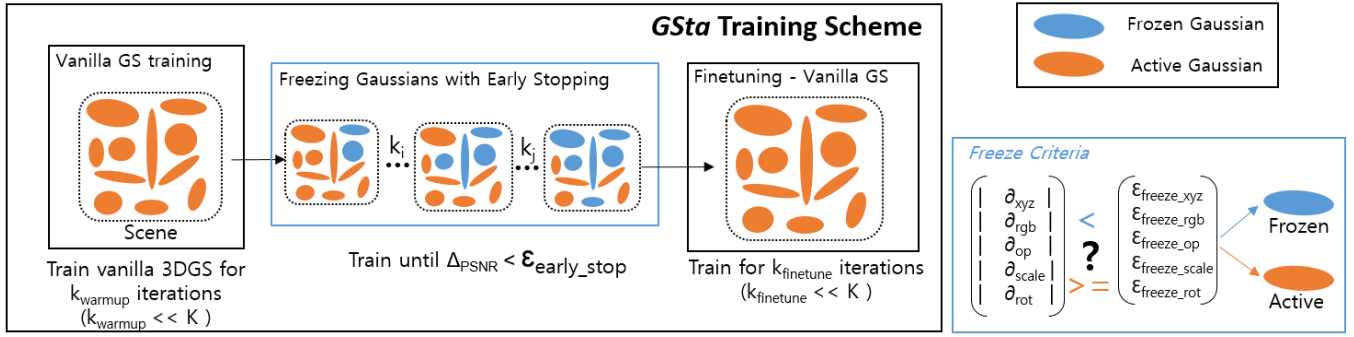
Fig. 2: Our proposed GSta training strategy. During training, we observe the gradients of Gaussian parameters (position *xyz* and color *rgb* used in practice) to decide which Gaussians have converged. We then progressively freeze (e.g. stop training) converged Gaussians, until we either hit our proposed training-set based early stopping criteria, or finish training. We then *unfreeze* all Gaussians and finetune them for a few iterations for global alignment. GSta leads to reduced training time, disk size and peak memory consumption.

(e.g. some converging earlier than others), we exploit this to improve training efficiency. An insignificant number of Gaussians remain with high gradients after early stages of training. We infer this by visualising the mean gradient magnitude, Figure 1, and the maximum gradient magnitudes over all Gaussians. While the mean gradient magnitudes converge around 5K iterations, we could measure the variance of the magnitudes varies in later stages of the training. Based on the norms of the color and positional gradients of Gaussians during training, we force some of the Gaussians (which have gradient norms below a threshold) to take a *siesta*, and freeze them for the next iterations of the training. This gradually decreases the overall gradient flow to calculate and optimize, improving training efficiency. Second, we introduce a simple but effective early stopping method for GS training. Unlike methods which use testing images for early stopping validation, we observe that using a subset of training images work equally well, if not slightly better. This facilitates a *fairer* early stopping as we do not tune model weights on the test images. Third, we introduce improvements for a more stable training, such as learning rate schedulers and using dynamic thresholds for gradient thresholding within adaptive densification and freezing. We also investigate the use of gradients from diffused colors together with the positional gradients which improve the overall effectiveness of the training wit a lower number of Gaussians.

We evaluate GSta on multiple datasets and integrate it with other methods, showing that it can improve the vanilla model as well as another efficient GS method (Trick-GS [18]). Our approach works well with orthogonal techniques for improving efficiency and our contributions are as follows:

- We propose GSta, a gradient-based method that dynamically identifies Gaussians that are close to convergence, and freezes them for the rest of the training. This helps improve training speed, without hurting accuracy.
- Alongside GSta, we introduce a global finetuning stage, where we force all Gaussians out of their *siesta* to globally align them for better results.
- We propose a training-set based early stopping method, where we end the training if performance on a randomly chosen subset of training images saturate. This helps improve the training speed.

- We show that GSta works well with existing GS methods, as well as other efficiency-improving techniques. Our results on three datasets show substantial gains in training time, disk size and peak memory consumption, while having competitive accuracy.

II. RELATED WORK

Neural 3D Reconstruction. NeRF approaches, where the appearance and geometry of a scene are encoded into the weights of a small neural network, have been popularized thanks to their compact representation as well as high-quality results. Despite the advances made in the efficiency of NeRF methods [8]–[10], NeRFs rely on the expensive ray marching process, which inevitably increases the runtime. Gaussian Splatting methods [5] does away with ray marching; they represent the scene with 3D Gaussian primitives and perform blending in screen space, speeding up the rendering process quite significantly. Despite their popularity, GS methods suffer from high storage and training memory requirements, since scenes are represented with over million of Gaussian primitives. This also translates to sub-optimal training times, and rendering speeds that can still be improved.

Improving Storage Efficiency. The storage footprint of GS methods rely on two major factors; number of Gaussians used to represent the scene and the 59 primitives that make up a Gaussian. There are several methods targeting to address the former by assigning a significance score [19]–[21] to each Gaussian to eliminate the insignificant ones; [11] computes significance on how frequently a Gaussian comes up in a training view, [16] learns a significance value during training, [22] removes Gaussians with significant overlap to its neighbors, [14] removes 3% of lowest-opacity Gaussians, [15] performs a fine-tuning stage for pruning and [23] explicitly enforces sparsity among Gaussians. Some methods address the latter, where [11], [14], [16], [24], [25] propose to reduce/mask/replace spherical harmonic bands and [16] leverages a hash-grid to compress color parameters. Parallel to these two lines of work, attribute compression via Vector Quantization [11], [16], [26], bit-quantization [26], [27] and leveraging entropy constraints [26], [28]–[31] are shown to be effective for storage footprint reduction. A final line of work focus on structural relationships between Gaussians in a scene, and propose anchors [32]–[35] from which Gaussians

can be derived efficiently. Mapping Gaussian attributes to 2D grids [13], adopting efficient data structures like octrees [36] and tri-planes [37], using Gaussians' spatial positions for improved organization [24], [38] and leveraging selective rendering [22] are some examples.

Improving Training Efficiency. Similar to NeRFs, Gaussian Splatting methods often require per-scene training, which makes training efficiency a critical factor. Most methods that improve storage efficiency also tend to improve training efficiency, therefore we will not mention them separately here. Other methods, such as [39] accelerating atomic operations in raster-based differential rendering, separation of SH bands into different tensors to load to rasterizer separately [40], densification based on position and appearance criteria [41], organization of Gaussians into manageable groups [42] and introduction of visibility culling [43] have shown training speed improvements.

A similar line of work to ours is [41], where authors leverage positional or appearance gradients for densification. Our work differs from theirs in several key aspects; we i) use positional and appearance gradients jointly, ii) use them for freezing Gaussians during training, not just for densification, iii) propose a finetuning stage for global optimization of frozen Gaussians, iv) leverage PSNR values of a subset of training images for early stopping and v) propose other minor tricks, such as using new optimizers and learning rate schedulers. GSta is a plug-and-play improvement that can improve several GS methods and it complements other efficiency-improving approaches.

III. METHODOLOGY

In this section, we first give preliminary information on 3DGS and later describe our method in detail.

A. Preliminaries

3DGS performs 3D reconstruction by learning a number of 3D Gaussian primitives, which are rendered in a differentiable volume splatting rasterizer [44]. A scene/object is often represented with up to several millions of Gaussians, where each Gaussian consists of 59 parameters. The 2D Gaussian G_i' projected from a 3D Gaussian G_i is defined as

$$G_i'(x) = e^{-\frac{1}{2}(x-\mu_i')^T \Sigma_i'^{-1}(x-\mu_i')}, \tag{1}$$

where μ_i is the 3D position, x is the position vector, and Σ_i is the 3D covariance matrix which is parameterized via a scaling matrix S and a rotation matrix (represented in quaternions q). $'$ indicates the 2D re-projection of respective parameters. Each Gaussian has an opacity ($\alpha \in [0,1]$), a diffused color and a set of spherical harmonics (SH) coefficients (up to 3 bands) that represent view-dependent color information. Color C of each pixel is determined by N Gaussians contributing to that pixel, where their colors are blended in a sorted order within the volumetric rendering regime. Color C is calculated as

$$C = \sum_{i \in N} c_i \alpha_i \prod_{j=1}^{i-1}(1-\alpha_j), \tag{2}$$

where c_i and α_i are the view-dependent color and opacity of a Gaussian. respectively. The standard L1 reconstruction loss and SSIM loss is used for training, and Gaussians are pruned and densified based on their gradient norms and opacity values.

Gaussians are initialized from a point-cloud calculated from SfM [45] methods, and they are iteratively updated based on the gradient descent algorithm, where training views of a scene are rendered. The attributes of Gaussians are updated with the calculated gradients based on ℓ_1 norm of the rendered output, $\mathcal{L}_1$, and its structural similarity, $\mathcal{L}_{\text{D-SSIM}}$ with the ground-truth image. The final loss is calculated as in Eq.3 to obtain a well represented scene reconstruction until K^{th} training iteration. The overall loss is defined as

$$\mathcal{L} = (1 - \lambda_{SSIM})\mathcal{L}_1 + \lambda_{SSIM}\mathcal{L}_{\text{D-SSIM}}, \tag{3}$$

where $\lambda_{SSIM} = 0.2$.

B. Efficient training scheme

Our proposed scheme is based on the observation that Gaussians have different convergence rates during training. Figure 1 shows the mean magnitude of all Gaussians during the training of "bicycle" scene of MipNeRF-360 [46] dataset. It can be observed that most Gaussians do converge early, however the densification stage still continues to add more Gaussians, due to some Gaussians (e.g. ones that did not yet converge) still having high gradients. This supports the fact that a large number of Gaussians do not need to be trained (e.g. frozen) further, and we can just continue training (e.g. unfrozen) the rest that have high gradients. The frozen Gaussians should ideally be unfrozen at some point, since the reconstruction quality will change with the updated Gaussians, and the frozen Gaussians might need to be updated to align with the new fitting. We detail our overall algorithm in Algorithm 1.

1) Leveraging gradients for efficient GS training: Vanilla 3DGS uses positional parameters and their gradients for its densification process. In GSta, we use a similar strategy for efficient training, and take action depending on magnitude of the chosen parameters' gradients. More specifically, GSta freezes the parameters of Gaussians' during training, if the magnitude of the parameters' gradient is lower than a threshold. We use positional and diffused color parameters' gradients for this purpose. Additionally, we freeze Gaussians only when they have low magnitude gradients on both color and positional parameters, and not just one of them.

Vanilla GS uses fixed threshold values to decide which Gaussians need to be densified or not, based on their gradient magnitudes. GSta, on the other hand, dynamically changes the thresholds that are used to decide which Gaussians to be frozen. We enforce the thresholds for color and positional parameters $p \in \{xyz, rgb\}$ to be between $\lambda_{freeze,1} * \epsilon_{k,freeze}^p$ and $\lambda_{freeze,2} * \epsilon_{k,freeze}^p$, where $\lambda_{freeze,1} = 0.5, \lambda_{freeze,2} = 1.5$. We gradually increase the thresholds proportional to current training iteration k until the training hits an early stopping criteria (see Sec. III-B.2) or until the adaptive densification stops, as we aim to freeze less Gaussians in

early stages of the training and freeze more as the number of Gaussians increase.

A Gaussian's gradients are calculated during backpropagation and corresponding weights are updated only if Gaussian's freeze criteria, $freeze_i^p$ is set to false, which is decided as

$$freeze_i^p = \begin{cases} True, & \|grad_i^p\| < \epsilon_{k,freeze}^p \\ False, & \text{otherwise,} \end{cases} \quad (4)$$

where k is the current training iteration and $\|grad_i^p\|$ is magnitude of the gradient for p^{th} parameter of ith Gaussian. $\epsilon_{k,freeze}^p$ is a threshold chosen for the current training iteration k and for the specific Gaussian parameter p, which is calculated as

$$\epsilon_{k,freeze}^p = \lambda_{freeze,1} * \epsilon_{k-1,freeze}^p + \\ k/K * \lambda_{freeze,2} * \epsilon_{k-1,freeze}^p \quad (5)$$

During training, GSta freezes a Gaussian, G_i only if both $freeze_i^{xyz}$ and $freeze_i^{rgb}$ is $True$.

$$freeze_i = \begin{cases} True, & freeze_i^{xyz} \text{ and } freeze_i^{rgb} \\ False, & \text{otherwise,} \end{cases} \quad (6)$$

where $freeze_i$ is the freeze map at iteration i (see Figure 2 for a visualization).

2) Early stopping: Most GS models are trained with fixed number of training iterations. An efficient GS training strategy requires to be aware of convergence. Therefore, we adopt early stopping strategy based on accuracy metrics, such as $PSNR$. We enforce the early stopping of GSta's freezing strategy and enable all Gaussians to be updated for K_f number of finetuning iterations. This early stopping is invoked if the change in $PSNR$ metric for the kth training iteration, $\Delta PSNR_k$, is lower than a threshold, ϵ_{PSNR} value.

However, calculating the $PSNR$ at every training iteration is costly and therefore, we update the metric every K_{PSNR} iterations. We also use a patience factor (wait count) of 1 and require the early stopping criteria to be met twice to define a more reliable convergence criteria. We define the early stopping criteria as

$$\text{early\_stop} = \begin{cases} \text{True,} & \Delta PSNR_k < \epsilon_{PSNR} \text{ and} \\ & \Delta PSNR_{k-K_{PSNR}} < \epsilon_{PSNR}, \\ \text{False,} & \text{otherwise,} \end{cases} \quad (7)$$

Note that we do not use the test images for early stopping, which means we do not tune the model based on the test accuracy. Instead, we observe that using the training images for this purpose gives equally good results, which makes it *fairer* than tuning model parameters on the test set itself.

3) Learning Rate Scheduling: Vanilla GS is trained with a learning rate for the positional parameters with a cosine decay factor and fixed learning rates for the other parameters. We observe that the final accuracy is highly sensitive to the learning rates and their decay factor. Therefore, we use a learning rate scheduler, which helps us guarantee convergence with the early stopping criteria. More specifically, we use a plateau learning rate scheduler based on the $PSNR$

metric and decay the learning rate of the positional Gaussian parameter with a factor, d. The plateau is decided based on threshold value of $\epsilon_{LR-PSNR}$ and a patience factor of 1.

4) Rasterizer & optimizer: The vanilla rasterizer in 3DGS is implemented to calculate gradients propagated from the pixels to the Gaussians. However, we need to propagate the gradients per Gaussian during the backward pass, since GSta adopts per splat based freezing strategy. Taming-3DGS [40] proposes a parallelization scheme per tile over the 2D splats. Their rasterizer makes better use of storing per-splat state and continually exchange per-pixel states between the threads. Hence, we make use of the per splat based rasterizer [40] and modify it to use our freeze maps. The modified rasterizer bypasses the gradient calculation in the backward pass, if the Gaussian's, G_i, freeze map label, $freeze_i$, is set to $False$.

Since the gradients are not calculated for some Gaussians, the optimizer is not going to update any parameters of those Gaussians. Therefore, we can also make use of a modified optimizer [40] to only update the Gaussian parameters if $freeze_i$ is set to $True$. Note that both these rasterizer and optimizer saves computational resources, which improves training efficiency and speed.

C. Adding Bag of Tricks for Increased Efficiency

Our proposed algorithm can reduce the training time by $6\times$, which includes the Gaussian freezing with early stopping strategy, learning rate scheduling and by using the proposed rasterizer and optimizer. We also make use of other, ideally orthogonal efficiency improvement methods along with GSta to push the frontier even further. We mostly use the tricks of Trick-GS [18]; readers are referred to the original work for further details. We explain each trick briefly below.

Pruning with Volume Masking. [13] learns masks for pruning the Gaussians with low scale and opacity. Hard masks, $M \in \{0,1\}^N$, are learned for N Gaussians and applied on their opacity and non-negative scale attributes by introducing a soft mask parameter, $m \in \mathbb{R}^N$ for each Gaussian. Introduced mask parameters are removed at the end of the training and do not add an extra storage cost. Hard masks can be extracted with $M_n = \text{sg}((\sigma(m_n) > \epsilon) - \sigma(m_n)) + \sigma(m_n)$, where sg is the stop gradient operator and σ is the sigmoid function. Soft masks are learned as a logistic regression problem.

Pruning with Significance of Gaussians. We adopt the significance based Gaussian pruning strategy proposed in [11]. Significance of the Gaussians are determined by considering all the rays passing through each training pixel and then by calculating how many times each Gaussian is hit. Scale and opacity of each Gaussian also contributes to the final score for each Gaussian. Finally, the scores are used to prune percentile of the whole set, starting with the Gaussians with lowest significance. This pruning strategy is applied only twice during training runs, since the score calculation for the whole set is costly.

Spherical Harmonic (SH) Masking. Almost 76% of Gaussian parameters are SH parameters of 3 SH bands. Therefore, they represent the arguably biggest bottleneck for achieving

low storage requirements. We choose a similar strategy to Gaussian masking [13] and SH bands pruning [27] for each Gaussian. Instead of learning a single soft mask parameter for each Gaussian, we learn 3 parameters corresponding to SH bands of a Gaussian. Instead of pruning SH bands, they are set to zero and used within the rasterizer. At the end of training, SH bands that are masked out are pruned and not saved, improving storage footprint. Note that we use SH masking only with $GSta + TrickGS + small$ (see Sec IV-B).

Progressive Training. Progressive training strategies help lower storage and training time by starting from a lower resolution image representation. Gradually increasing the resolution [28], [47] lets the optimization focus on low frequency details first and high frequency details at later iterations. We adopt a similar trick and starting from a lower resolution, we increase the resolution size with a cosine scheduler until 6K iterations.

Blur. Another way to make the optimization focus on low frequency details first is adding Gaussian blur [28] on the image. We add Gaussian blur on the original image by starting with a larger kernel size and gradually decay it with a cosine scheduler and remove the noise until 6K iterations.

Accelerated SSIM loss calculation. Another trick for training time efficiency is to modify $SSIM$ loss calculation with optimized CUDA kernels [40], where each 2D convolution kernels with in the calculation is replaced with two 1D kernels. Later a fused kernel from the output of 1D convolutions are used to calculate $SSIM$.

IV. Experimental Results

We first include details of our experimental setup and implementation, and then discuss our experimental evaluation and comparison with state of the art methods.

A. Experimental Setup and Implementation Details

Metrics and datasets. We evaluate our method on various bounded and unbounded indoor/outdoor scenes; Mip-NeRF-360 [46], Tanks&Temples [48] and DeepBlending [49] are used in our experiments. Following [5], we use the pre-computed point clouds and camera poses for training and use every 8th image for evaluation. We use the commonly used PSNR, SSIM and LPIPS metrics [50] for evaluating GSta. We train and evaluate our method on a single NVIDIA RTX 3090 and use *torch.cuda.Event* function to report training time (including densification), and provide FPS values as the average of 50 runs using *torch.utils.benchmark*. Note that we measure training times and FPS values on the same hardware, including Mini-Splatting-v2 and Taming-3DGS [40], [43].

GSta Details. GSta dynamically adjusts the thresholds used for the densification and freezing Gaussians. More specifically, thresholds are proportionally adjusted to the current training iteration and are scaled between $[0.5, 1.5]$ starting with their initial values. Initial thresholds for the densification are set to $eps\_den\_xyz = 0.0002$ and $eps\_den\_rgb = 0.000001$. Initial thresholds for freezing Gaussians are set to $eps\_f\_xyz = 0.00003$ and $eps\_f\_rgb = 0.0001$. The thresholds are chosen once by observing the convergence

---

Algorithm 1 GSta: Efficient Training Iteration for 3DGS.

- G: Set of all Gaussian parameters, gt_image: ground-truth image, cam_pose: camera pose of gt_image.
- eval_image: evaluation images, eval_cam_pose: camera poses of eval_image, eval_freq: frequency of evaluation.
- total_iter: total train iterations, iter: current train iteration, psnrs: list of previous PSNRs.
- stop_p: early stopping patience, stop_eps: early stopping threshold, max_stop_it: early stopping max number of iterations.
- eps_f_xyz, eps_f_rgb: initial thresholds for xyz and rgb gradients for freezing.
- finetune: current finetuning state, ft_iter_rem: remaining finetuning iterations.

```
 1: while iter < total_iter or ft_iter_rem! = 0 do
             ▷ Train until max training or finetuning iteration is reached.
 2:     gt_image, cam_pose ← sample_batch();        ▷ Sample batch.
 3:     eps_f_xyz, eps_f_rgb ←      ▷ Freezing threshold value update.
 4:          update_epsilons(iter, total_iter, eps_f_xyz, eps_f_rgb);
 5:     early_stop ←              ▷ Early stopping based on PSNR values.
 6:          is_early_stop(psnrs, iter, stop_p, stop_eps, max_stop_it);
 7:     if early_stop = False AND finetune = False then
 8:         freeze_map ←      ▷ Update freeze map with new thresholds.
 9:             update_freeze_map(G, eps_f_xyz, eps_f_rgb);
10:     else if finetune = False then
          ▷ Early stop is True. Unfreeze all Gaussians, activate finetuning.
11:         freeze_map ← reset_freeze_map(G);
12:         finetune ← True;
13:     end if
          ▷ Periodically validate model to get PSNRs for early stopping.
14:     if iter%eval_freq = 0 and finetune = False then
15:         psnrs ← validate_model(G, eval_ims, eval_cam_pose);
16:     end if
17:     lr ← LR_scheduler(psnrs);                       ▷ Update LR.
18:     render_image ← rasterize(G, freeze_map, cam_pose);
19:     loss ← loss_fcn(gt_image, render_image);   ▷ Calculate loss.
20:     optimizer_step(G, lr, loss, freeze_map);
21:     G ← adaptive_densification(G);                      ▷ Densify.
22:     G ← opacity_reset(G);                      ▷ Reset opacities.
23:     if finetune = True AND ft_iter_rem > 0 then
24:         ft_iter_rem ← ft_iter_rem − 1;
25:     else if early_stop ← False OR iter < total_iter then
26:         iter ← iter + 1;
27:     end if
28: end while
```

---

of each parameters' gradient magnitudes and applied the same on all scenes. Freeze map is updated according to the current parameters' thresholds every 250 iterations and frozen Gaussians are accumulated until our algorithm meets early stopping criteria. It implies that if a Gaussian is frozen in the previous iterations it will stay frozen in later iterations. GSta unfreezes some Gaussians only if they would be pruned within the densification stage. We also reset the freeze map at every $k_{f_{reset}} = 2K$ iterations and do not start re-freezing until $k_{f_{wait}} = 500$ iterations pass to give chance for some Gaussians to be unfrozen later.

Our algorithm early stops and starts finetuning the representation if the change in PSNR is less than $0.2dB$ with a patience of 1 PSNR calculations, and we update models' current PSNR every $1K$ iterations until the freezing complete. GSta trains without freezing for $k_{warmup} = 3K$ iterations and activates the freezing algorithm between $[3K, \min(10K, early\_stop\_iter)]$ iterations. Although we train in full fp32 precision, we save and evaluate our models in reduced fp16 precision, which allows us to lower the storage size for practically no loss in accuracy.

Dataset	Mip-NeRF 360							Tanks&Temples						
Method	PSNR ↑	SSIM ↑	LPIPS ↓	Storage ↓ (MB)	Time ↓ (min)	Max-#GS ↓ ×1000	#GS ↓ ×1000	PSNR ↑	SSIM ↑	LPIPS ↓	Storage ↓ (MB)	Time ↓ (min)	Max-#GS ↓ ×1000	#GS ↓ ×1000
*INGP-base [8]	25.30	0.671	0.371	13	5.62	-	-	21.72	0.723	0.330	13	5.43	-	-
*INGP-big [8]	25.59	0.699	0.331	48	7.50	-	-	21.92	0.745	0.305	48	6.98	-	-
*Turbo-GS [41]	27.38	0.812	0.210	240	5.47	-	490	23.49	0.841	0.176	-	4.35	-	-
3DGS [5]	27.56	0.818	0.202	770	23.83	3265	3255	23.67	0.845	0.178	431	14.69	1824	1824
Mini-Splatting-v2 [43]	27.37	0.821	0.215	139	3.93	4744	618	23.16	0.842	0.185	84	2.35	3890	358
Taming-3DGS [40]	27.25	0.795	0.260	151	6.46	670	670	23.73	0.836	0.210	72	4.02	319	319
Trick-GS [18]	27.16	0.802	0.245	39	15.41	1369	830	23.48	0.830	0.209	20	10.56	696	443
GSta	27.21	0.812	0.227	304	7.89	2740	2699	22.90	0.833	0.203	165	3.99	1511	1468
GSta+Trick-GS+small	27.13	0.807	0.242	48	5.30	1774	1148	23.02	0.830	0.207	28	4.37	920	727
GSta+Trick-GS	27.14	0.807	0.241	130	4.84	1781	1159	23.13	0.832	0.202	103	2.89	1252	914

TABLE I: Quantitative evaluation on MipNeRF 360 and Tanks&Temples datasets. Results marked with "*" are taken from the corresponding papers. Results between the double horizontal lines are from retraining the models on our system. GSta can reconstruct scenes with low training time and very low disk space requirements, while achieving competitive accuracy.

Dataset	Deep Blending						
Method	PSNR ↑	SSIM ↑	LPIPS ↓	Storage ↓ (MB)	Time ↓ (min)	Max-#GS ↓ ×1000	#GS ↓ ×1000
*INGP-base [8]	23.62	0.797	0.423	13	6.52	-	-
*INGP-big [8]	24.96	0.817	0.390	48	8.00	-	-
*Turbo-GS [41]	30.41	0.910	0.240	-	3.24	-	-
3DGS [5]	29.46	0.899	0.266	664	25.29	2808	2808
Mini-Splatting-v2 [43]	30.19	0.912	0.240	73	3.16	5255	651
Taming-3DGS [40]	30.07	0.904	0.270	33	4.52	294	294
Trick-GS [18]	29.46	0.899	0.260	25	13.11	1308	639
GSta	29.40	0.906	0.251	296	7.37	2629	2629
GSta+Trick-GS+small	29.33	0.905	0.260	48	4.44	1877	1399
GSta+Trick-GS	29.41	0.906	0.257	158	4.68	1887	1405

TABLE II: Quantitative evaluation on Deep Blending dataset. Results marked with * are taken from the corresponding papers. Results below the double horizontal line are trained and evaluated on our system.

GSta uses the same learning rates as the vanilla model, except the opacity learning rate which is 0.025. Plateau learning rate schedulers are implemented with a learning rate decay factor of 0.75, patience of 1 and epsilon of 1.

We densify every 100 iterations starting from iteration $(500, \min(10K, early\_stop\_iter))$, and prune unnecessary Gaussians with the aforementioned pruning strategies. Similarly, opacity reset is applied from iterations $[3K, \min(10K, early\_stop\_iter)]$ with a step size of $3K$.

We additionally use a trick introduced in $Taming-GS$ [40] and replace the activation function of opacity from "sigmoid" to "absolute" activation function when finetuning of our method is activated. The regular capped Gaussian primitives are converted to high-opacity Gaussians which is shown to represent opaque surfaces with less number of Gaussians. Following Turbo-GS [41], we adopt gradients from diffused color parameters together with positional parameters. They are used both for adaptive densification and in our case, also for freezing. Gradients from diffused colors are activated 20% of the time to be used in densification and they are always used together with the positional based gradients for freezing Gaussians.

Trick-GS Details. We get inspiration from Trick-GS [18] for scheduling image resolutions, blurring and significance score based pruning. Starting from an image resolution with scale 0.175, we gradually increase it back to the original resolution until iteration $6K$ using a cosine scheduler. Similarly, Gaussian kernels are initialized to 5×5, and kernel size is adapted to correspond 0.25 of the image scales. Kernel size is gradually lowered with a $\log$ scheduler to remove the noise until iteration $6K$. Significance based pruning is applied at

iterations $4K$ and $7K$ with 75% of removal factor and a decay of 0.8. SH masks are learned only during finetuning iterations. We learn adaptive GS mask pruning from iteration $1K$ to $10K$ and prune Gaussians every $1K$ iterations. Please refer to [18] for the rest of the parameters as we keep the rest of settings the same.

B. Performance Evaluation

We compare GSta with four state of the art approaches, Mini-Splatting-v2 [43], Taming-GS [40], Trick-GS [18] and finally Turbo-GS [41]. We run all approaches on our system except Turbo-GS [41], as the implementation was not available on the day of this submission. We propose three variants of our model, $GSta$, $GSta+TrickGS$ and $GSta+TrickGS+small$, where the first is GSta applied on vanilla 3DGS, second is GSta combined with Trick-GS, and the third is essentially the second but with SH masking for even lower storage. The results are shown in Tables I and II.

Results. $GSta$ achieves competitive accuracy, while reducing the storage requirements and training times ~ 3 fold and improving peak number of Gaussians by 50% compared to vanilla GS. The results show that $GSta$ achieves faster training than $Trick-GS$ and has half the peak number of Gaussians of $Mini-Splatting-v2$. It has better accuracy (e.g. LPIPS) than $Taming-3DGS$, but exhibits slightly worse storage and peak memory performance. These results show that $GSta$ does improve the current state-of-the-art, and is preferable over others in different aspects; e.g. lower training memory than $Mini-Splatting-v2$, faster than $Trick-GS$ and more accurate than $Taming-3DGS$.

Combining with Trick-GS. $GSta + TrickGS$ presents further gains over $GSta$, where storage, training time and peak memory requirements are all reduced, with little to no drop in accuracy. Compared to vanilla GS on MipNeRF-360, $GSta+TrickGS$ reduces the storage by ~ 5, training time by ~ 5 and improves peak memory by up to a relative 60%. Similar to before, $GSta + TrickGS$ now converges even faster than $Trick-GS$, has less than half the peak memory of $Mini-Splatting-v2$ and now trains faster than $Taming-3DGS$. These trends also hold for the other two datasets, where the results show that $GSta$ not only is accurate itself, but also can also leverage orthogonal efficiency improvement methods, such as $Trick-GS$, to achieve even further gains.

Fig. 3: Qualitative comparison of the methods (top left to bottom right: 3DGS [5], Mini-Splatting-v2 [43], Taming-GS [40] and ours). Our method can recover more consistent background while keeping low training time and great storage compression rates. We show zoomed prediction images except GT.

$GSta + TrickGS + small$ presents our smallest model, to see how far we can go in achieving efficient GS. At the cost of some drop in accuracy, it introduces some drastic compression rates; it achieves $16\times$ reduction in storage, $5\times$ reduction in training time and $2\times$ reduction in peak memory compared to vanilla 3DGS on MipNerf-360, and similar rates of improvements on other datasets. $GSta + TrickGS + small$ has much less storage size than $Taming - 3DGS$ and $Mini - Splatting - v2$, better training time than $Taming - 3DGS$ and significantly lower peak memory consumption than $Mini - Splatting - v2$. In overall, the results show that GSta advances the efficiency-fidelity frontier further and takes a decisive step towards edge-friendly GS systems.

Qualitative Results. Images in Figure 3 show that our method is highly accurate. $Taming - 3DGS$, and $MiniSplatting - v2$ to a certain extent, fail to capture high-frequency details (e.g. tree leaves in both images), whereas our method successfully captures complex details and has no visible difference in quality compared to vanilla 3DGS.

C. Ablation Study

We now analyze the impact of GSta and its components. We do so by progressively removing components from GSta, and see their individual effect. The results of our analysis are shown in Table III.

Freezing strategies. We first analyse whether our freezing strategy does improve on two naive approaches; randomly freezing 25% (*random*) of Gaussians or freezing ones with lowest 25% gradients (*mingrad*). The results (rows 3, 8 and 9) show that our freezing strategy (GSta) has the best training time. Furthermore, *random* introduces drops in accuracy, as it tends to end training with fewer Gaussians than others because it randomly freezes Gaussians with high gradient magnitudes. Row 3 shows that not using any freezing has the worst training time among others, showing the value of our Gaussian freezing approach. Finally, we evaluate the GSta model without the freeze module trains even slower than using a freeze module with random selections.

LR scheduler and dynamic thresholding. The addition of LR scheduler (rows 5) shortens the training time by 2 minutes but has no tangible effect on other metrics. The introduction of dynamic thresholding (row 7) in our freezing

Dataset	MipNeRF360 - bicycle						
Method	PSNR ↑	SSIM ↑	LPIPS ↓	Storage ↓ (MB)	Time ↓ (min)	Max-#GS ↓ ×1000	#GS ↓ ×1000
GSta+TrickGS	25.23	0.758	0.248	223	5.0	2512	1982
GSta+Trick-GS+small	25.20	0.756	0.248	82	5.6	2507	1981
GSta	25.12	0.759	0.235	457	6.4	4075	4060
GSta-freezing	25.16	0.764	0.212	427	15.7	3974	3795
GSta-lrscheduler	25.17	0.762	0.229	454	11.3	4041	4036
GSta-rgb	25.18	0.755	0.239	509	8.9	4542	4520
GSta-dynamic	25.15	0.758	0.239	443	7.8	3933	3933
GSta+mingrad	25.25	0.765	0.223	434	9.0	3981	3855
GSta+random	25.02	0.748	0.241	353	13.1	3323	3140
3DGS	25.21	0.767	0.205	713	37.6	6331	6331

TABLE III: Ablation study on different components of our model. "-" indicates the removal of a component (e.g. -freezing means no freezing) and similarly "+" indicates additional modules (e.g. +small means with SH masking). *mingrad* and *random* are alternative ways of freezing (see Section IV-C).

strategy and densification strategy shows improvements in training time as well, showing its practical usefulness.

Gradient information. We now analyse the need both rgb and xyz gradients in our freezing approach. Rows 6 shows that only using xyz both harms training time, storage and peak memory. This shows the practical value of rgb gradients in being a proxy for a Gaussian's usefulness.

Trick-GS. $Trick - GS$ techniques synergizes very well with our GSta (see rows 2 and 3), where huge gains in storage and peak memory are observed, as well as slight gains in training time, with virtually no drop in accuracy metrics.

V. Conclusion

On device learning of GS is costly and it requires efforts on multiple evaluation metrics, such as accuracy, training time, storage requirement. In this work, we propose GSta, a generic training scheme for 3DGS that can be used as a plug-and-play module for any GS-based method. Consisting of a novel Gaussian freezing scheme, early stopping mechanism and improved hyper-parameter selections, GSta advances the frontier of efficient GS methods on multiple fronts, such as training memory, time and storage requirements, while preserving competitive accuracy.

References

[1] M. Adamkiewicz, T. Chen, A. Caccavale, R. Gardner, P. Culbertson, J. Bohg, and M. Schwager, "Vision-only robot navigation in a neural radiance world," *IEEE Robotics and Automation Letters*, vol. 7, no. 2, pp. 4606–4613, 2022.

[2] K. Georgiadis, M. K. Yucel, and A. Saa-Garriga, "Cheapnvs: Real-time on-device narrow-baseline novel view synthesis," *arXiv preprint arXiv:2501.14533*, 2025.

[3] E. Skartados, M. K. Yucel, B. Manganelli, A. Drosou, and A. Saà-Garriga, "Finding waldo: Towards efficient exploration of nerf scene spaces," in *Proceedings of the 15th ACM Multimedia Systems Conference*, 2024, pp. 155–165.

[4] S. Li, C. Li, W. Zhu, B. Yu, Y. Zhao, C. Wan, H. You, H. Shi, and Y. Lin, "Instant-3d: Instant neural radiance field training towards on-device ar/vr 3d reconstruction," in *Proceedings of the 50th Annual International Symposium on Computer Architecture*, 2023, pp. 1–13.

[5] B. Kerbl, G. Kopanas, T. Leimkühler, and G. Drettakis, "3d gaussian splatting for real-time radiance field rendering," *ACM Transactions on Graphics*, vol. 42, no. 4, July 2023.

[6] B. Cyganek and J. P. Siebert, *An introduction to 3D computer vision techniques and algorithms*. John Wiley & Sons, 2011.

[7] B. Mildenhall, P. P. Srinivasan, M. Tancik, J. T. Barron, R. Ramamoorthi, and R. Ng, "Nerf: Representing scenes as neural radiance fields for view synthesis," *Communications of the ACM*, vol. 65, no. 1, pp. 99–106, 2021.

[8] T. Müller, A. Evans, C. Schied, and A. Keller, "Instant neural graphics primitives with a multiresolution hash encoding," *ACM Transactions on Graphics*, vol. 41, no. 4, pp. 1–15, 2022.

[9] C. Reiser, S. Peng, Y. Liao, and A. Geiger, "Kilonerf: Speeding up neural radiance fields with thousands of tiny mlps," in *Proceedings of the IEEE/CVF international conference on computer vision*, 2021, pp. 14 335–14 345.

[10] A. Yu, R. Li, M. Tancik, H. Li, R. Ng, and A. Kanazawa, "Plenoctrees for real-time rendering of neural radiance fields," in *Proceedings of the IEEE/CVF international conference on computer vision*, 2021, pp. 5752–5761.

[11] Z. Fan, K. Wang, K. Wen, Z. Zhu, D. Xu, and Z. Wang, "Lightgaussian: Unbounded 3d gaussian compression with 15x reduction and 200+ fps," *arXiv preprint arXiv:2311.17245*, 2024.

[12] A. Hanson, A. Tu, V. Singla, M. Jayawardhana, M. Zwicker, and T. Goldstein, "Pup 3d-gs: Principled uncertainty pruning for 3d gaussian splatting," *arXiv preprint arXiv:2406.10219*, 2024.

[13] W. Morgenstern, F. Barthel, A. Hilsmann, and P. Eisert, "Compact 3d scene representation via self-organizing gaussian grids," in *Proceedings of European Conference on Computer Vision*, 2024.

[14] P. Papantonakis, G. Kopanas, B. Kerbl, A. Lanvin, and G. Drettakis, "Reducing the memory footprint of 3d gaussian splatting," *Proceedings of the ACM on Computer Graphics and Interactive Techniques*, vol. 7, no. 1, pp. 1–17, May 2024.

[15] M. S. Ali, M. Qamar, S.-H. Bae, and E. Tartaglione, "Trimming the fat: Efficient compression of 3d gaussian splats through pruning," *arXiv preprint arXiv:2406.18214*, 2024.

[16] J. C. Lee, D. Rho, X. Sun, J. H. Ko, and E. Park, "Compact 3d gaussian representation for radiance field," in *Proceedings of the IEEE/CVF Conference on Computer Vision and Pattern Recognition*, 2024, pp. 21 719–21 728.

[17] Z. Chen, F. Wang, Y. Wang, and H. Liu, "Text-to-3d using gaussian splatting," in *Proceedings of the IEEE/CVF conference on computer vision and pattern recognition*, 2024, pp. 21 401–21 412.

[18] A. Armagan, A. Saà-Garriga, B. Manganelli, M. Nowak, and M. K. Yucel, "Trick-gs: A balanced bag of tricks for efficient gaussian splatting," *arXiv preprint arXiv:2501.14534*, 2025.

[19] Y. Liu, Z. Zhong, Y. Zhan, S. Xu, and X. Sun, "Maskgaussian: Adaptive 3d gaussian representation from probabilistic masks," *arXiv preprint arXiv:2412.20522*, 2024.

[20] A. Hanson, A. Tu, V. Singla, M. Jayawardhana, M. Zwicker, and T. Goldstein, "Pup 3d-gs: Principled uncertainty pruning for 3d gaussian splatting," *arXiv preprint arXiv:2406.10219*, 2024.

[21] B. Zoomers, M. Wijnants, I. Molenaers, J. Vanherck, J. Put, L. Jorissen, and N. Michiels, "Progs: Progressive rendering of gaussian splats," *arXiv preprint arXiv:2409.01761*, 2024.

[22] Y. Seo, Y. S. Choi, H. S. Son, and Y. Uh, "Flod: Integrating flexible level of detail into 3d gaussian splatting for customizable rendering," *arXiv preprint arXiv:2408.12894*, 2024.

[23] Y. Zhang, W. Jia, W. Niu, and M. Yin, "Gaussianspa: An "optimizing-sparsifying" simplification framework for compact and high-quality 3d gaussian splatting," *arXiv preprint arXiv:2411.06019*, 2024.

[24] S. Shin, J. Park, and S. Cho, "Locality-aware gaussian compression for fast and high-quality rendering," *arXiv preprint arXiv:2501.05757*, 2025.

[25] Y. Wang, S. Chen, and R. Yi, "Sg-splatting: Accelerating 3d gaussian splatting with spherical gaussians," *arXiv preprint arXiv:2501.00342*, 2024.

[26] S. Niedermayr, J. Stumpfegger, and R. Westermann, "Compressed 3D gaussian splatting for accelerated novel view synthesis," in *Proceedings of the IEEE/CVF Conference on Computer Vision and Pattern Recognition*, 2024, pp. 10 349–10 358.

[27] H. Wang, H. Zhu, T. He, R. Feng, J. Deng, J. Bian, and Z. Chen, "End-to-end rate-distortion optimized 3d gaussian representation," in *Proceedings of European Conference on Computer Vision*, 2024.

[28] S. Girish, K. Gupta, and A. Shrivastava, "EAGLES: Efficient accelerated 3d gaussians with lightweight encodings," in *Proceedings of European Conference on Computer Vision*, 2024.

[29] M. S. Ali, S.-H. Bae, and E. Tartaglione, "Elmgs: Enhancing memory and computation scalability through compression for 3d gaussian splatting," *arXiv preprint arXiv:2410.23213*, 2024.

[30] S. Xie, W. Zhang, C. Tang, Y. Bai, R. Lu, S. Ge, and Z. Wang, "MesonGS: Post-training compression of 3d gaussians via efficient attribute transformation," in *Proceedings of European Conference on Computer Vision*, 2024.

[31] L. Liu, Z. Chen, and D. Xu, "Hemgs: A hybrid entropy model for 3d gaussian splatting data compression," *arXiv preprint arXiv:2411.18473*, 2024.

[32] T. Lu, M. Yu, L. Xu, Y. Xiangli, L. Wang, D. Lin, and B. Dai, "Scaffold-gs: Structured 3d gaussians for view-adaptive rendering," in *Proceedings of the IEEE/CVF Conference on Computer Vision and Pattern Recognition*, 2024, pp. 20 654–20 664.

[33] Y. Chen, Q. Wu, J. Cai, M. Harandi, and W. Lin, "Hac: Hash-grid assisted context for 3d gaussian splatting compression," in *Proceedings of European Conference on Computer Vision*, 2024.

[34] Y. Wang, Z. Li, L. Guo, W. Yang, A. C. Kot, and B. Wen, "Contextgs: Compact 3d gaussian splatting with anchor level context model," *arXiv preprint arXiv:2405.20721*, 2024.

[35] X. Liu, X. Wu, P. Zhang, S. Wang, Z. Li, and S. Kwong, "CompGS: Efficient 3d scene representation via compressed gaussian splatting," in *ACM Multimedia 2024*, 2024.

[36] K. Ren, L. Jiang, T. Lu, M. Yu, L. Xu, Z. Ni, and B. Dai, "Octree-gs: Towards consistent real-time rendering with lod-structured 3d gaussians," *arXiv preprint arXiv:2403.17898*, 2024.

[37] M. Wu and T. Tuytelaars, "Implicit gaussian splatting with efficient multi-level tri-plane representation," *arXiv preprint arXiv:2408.10041*, 2024.

[38] G. Fang and B. Wang, "Mini-splatting: Representing scenes with a constrained number of gaussians," in *Proceedings of European Conference on Computer Vision*, 2024.

[39] S. Durvasula, A. Zhao, F. Chen, R. Liang, P. K. Sanjaya, and N. Vijaykumar, "Distwar: Fast differentiable rendering on raster-based rendering pipelines," *arXiv preprint arXiv:2401.05345*, 2023.

[40] S. S. Mallick, R. Goel, B. Kerbl, F. V. Carrasco, M. Steinberger, and F. D. L. Torre, "Taming 3dgs: High-quality radiance fields with limited resources," *arXiv preprint arXiv:2406.15643*, 2024.

[41] T. Lu, A. Dhiman, R. Srinath, E. Arslan, A. Xing, Y. Xiangli, R. V. Babu, and S. Sridhar, "Turbo-gs: Accelerating 3d gaussian fitting for high-quality radiance fields," *arXiv preprint arXiv:2412.13547*, 2024.

[42] C. Wang, G. Ma, Y. Xue, and Y. Lao, "Faster and better 3d splatting via group training," *arXiv preprint arXiv:2412.07608*, 2024.

[43] G. Fang and B. Wang, "Mini-splatting2: Building 360 scenes within minutes via aggressive gaussian densification," *arXiv preprint arXiv:2411.12788*, 2024.

[44] M. Zwicker, H. Pfister, J. Van Baar, and M. Gross, "Ewa volume splatting," in *Proceedings Visualization*. IEEE, 2001, pp. 29–538.

[45] J. L. Schönberger and J.-M. Frahm, "Structure-from-motion revisited," in *Proceedings of the IEEE/CVF Conference on Computer Vision and Pattern Recognition*, 2016.

[46] J. T. Barron, B. Mildenhall, D. Verbin, P. P. Srinivasan, and P. Hedman, "Mip-nerf 360: Unbounded anti-aliased neural radiance fields," in *Proceedings of the IEEE/CVF Conference on Computer Vision and Pattern Recognition*, 2022, pp. 5470–5479.

[47] Z. Yang, X. Gao, Y. Sun, Y. Huang, X. Lyu, W. Zhou, S. Jiao, X. Qi, and X. Jin, "Spec-gaussian: Anisotropic view-dependent appearance for 3d gaussian splatting," *arXiv preprint arXiv:2402.15870*, 2024.

[48] A. Knapitsch, J. Park, Q.-Y. Zhou, and V. Koltun, "Tanks and temples: Benchmarking large-scale scene reconstruction," *ACM Transactions on Graphics*, vol. 36, no. 4, 2017.

[49] P. Hedman, J. Philip, T. Price, J.-M. Frahm, G. Drettakis, and G. Brostow, "Deep blending for free-viewpoint image-based rendering," *ACM Transactions on Graphics*, vol. 37, no. 6, pp. 1–15, 2018.

[50] R. Zhang, P. Isola, A. A. Efros, E. Shechtman, and O. Wang, "The unreasonable effectiveness of deep features as a perceptual metric," in *Proceedings of the IEEE/CVF Conference on Computer Vision and Pattern Recognition*, 2018, pp. 586–595.